Scientia Iranica B (2012) 19 (2), 311–319

Sharif University of Technology

Scientia Iranica

Transactions B: Mechanical Engineering

www.sciencedirect.com

High speed contouring enhanced with C^2 PH quintic spline curves

J. Jahanpour *

Department of Mechanical Engineering, Mashhad branch, Islamic Azad University, Mashhad, P.O. Box 9187147578, Iran

Received 19 June 2011; revised 23 November 2011; accepted 25 February 2012

KEYWORDS

PH curves;
B-spline curves;
Nodal points;
CNC interpolators;
Variable feedrate control;
Contour error.

Abstract This paper presents a C^2 Pythagorean-Hodograph (PH) spline curve interpolator for high speed contouring applications. With the knot vector and control points given, the C^2 PH quintic spline curve is a "good" interpolant to the nodal points of the cubic *B*-spline curve, with the same knot vector and control points. To generate the C^2 PH quintic spline curves, a uniform knot sequence is employed. The *S*-curve motion planning architecture, with variable feedrate for a planar C^2 PH quintic spline curve, is also developed. In particular, C^1 cubic feed acceleration/deceleration is imposed on the first and last PH quintic spline segments. Several closed C^2 PH quintic spline curve contouring tasks, along with a simple position loop controller, were conducted to verify the effectiveness of the proposed interpolation algorithm. The experimental results were analyzed and discussed. It is found that the proposed CNC interpolator is not only feasible for machining the complicated parametric curves represented in the C^2 PH quintic spline form, but also yields a satisfactory contouring performance for variable feedrate control.

1. Introduction

Development of parametric interpolator and feed acceleration/deceleration motion planning schemes is an important subject in CAD/CAM systems. Although several interpolators have been proposed for the standard free-form parametric curves, e.g. splines and NURBS (Non-uniform rational *B*-spline) [1–5], most of them rely on numerical integration (Taylor's expansion or the Runge–Kutta method) to compute the arc length. As a result, it is not possible to obtain the exact arc length information using those approaches, which makes interpolation, inherently, a rough approximation (even at fixed feedrates) [6]. The inaccurate arc length calculation results in fluctuation in the desired feedrate. To cope with this problem, Tsai and Cheng [7] proposed a Predictor–Corrector Interpolator (PCI) for NURBS curves, while Erkorkmaz and Altintas [1] developed an iterative interpolation technique for spline curves.

* Tel.: +98 511 6625046; fax: +98 511 6627560.
E-mail address: jahanpourfr@mshdiau.ac.ir.

1026-3098 © 2012 Sharif University of Technology. Production and hosting by Elsevier B.V. Open access under CC BY-NC-ND license.
Peer review under responsibility of Sharif University of Technology.

doi:10.1016/j.scient.2012.02.017

Production and hosting by Elsevier

Pythagorean Hodograph (PH) curves, which were first introduced by Farouki and Sakkalis [8] in 1990, are a special family of free-form parametric curves and a subset of the Bezier representation. In contrast to the conventional arc length parameterization, the arc length of a PH curve can be computed precisely by evaluating a polynomial function of the curve parameter [9,10]. Therefore, there is no feedrate fluctuation during interpolation. The fact that the PH curve has a polynomial representation, along with a special algebraic structure, makes it well suited for real-time CNC interpolation algorithms. For example, the feedrate can be fixed or specified as a function of cumulative arc length or local curvature along curved tool paths [11–13]. Besides, Tsai et al. [14] developed a closed-form solution for the interpolation integral using the *S*-curve [15–17] variable feedrate for a PH curve.

In general, a single PH curve cannot represent complicated open and closed shapes. Nevertheless, the aforementioned difficulties can be circumvented by connecting several PH segments together, which is called a PH spline curve. Several researchers have focused on PH spline curves and their applications [18–21]. For instance, Aigner et al. [18] studied the problem of approximating a given set of data points by PH spline curves. They formulated an evolution process within the family of PH spline curves to solve the highly non-linear curve fitting problem. Sir and Jutler [19] constructed a C^2 PH spline curve of degree nine using the C^2 Hermite data on an analytical curve. In [19], the C^2 Hermite data were assumed to be taken from a small segment of an analytical curve. An iteration technique was introduced to convert an analytical curve into a piecewise PH curve of degree nine. Accordingly, the parameter domain

of the analytical curve was split into 2^n uniform subintervals to obtain the C^2 Hermite data, i.e., the end points and their first- and second-order derivatives for all PH segments. The C^2 PH Hermit interpolant have significant advantages for practical design and manufacturing problems of cams [13,22], which require continuity in the follower displacement, velocity, and acceleration profiles. The PH spline curves not only inherit all the geometrical properties of the *B*-spline curves (e.g. strong convex hull and local shape modification properties), but also contain all the advantages of the PH curves. In addition, the PH spline curves provide significant advantages over ordinary polynomial curves in CAD/CAM applications, that is, they typically exhibit a better curvature distribution profile than the corresponding spline curve when interpolating a sequence of points [20,21].

Recently, several approaches have been developed in the design of PH spline curves through the use of control polygons of the *B*-spline and NURBS curves [20,23]. In both [20,23], the nodal points, which are the points on the curve corresponding to the specified knot points, are employed to construct the open and closed C^2 PH spline curves. In [20], the C^2 PH spline curve associated with given control points and a knot vector was defined to interpolate the nodal points of the cubic *B*-spline curve specified by the same control polygon and knots, while the C^2 PH spline curve of degree nine proposed in [23] was defined to interpolate the Hermit data obtained from the NURBS curve of degree three, specified by the given control polygon, weights, and knots.

The problem of constructing a C^2 PH quintic spline to interpolate a sequence points of $q_0, \ldots, q_M$ with related end-conditions is equivalent to solving a tridiagonal system of quadratic equations with complex unknowns [20,21]. Several analytical and numerical techniques useful for solving wide classes of nonlinear systems of equations, as well as nonlinear differential equations, have been focused in [21,24–27]. For instance, the numerical homotopy procedure determines all solutions – real or complex – to a given system of M non-linear equations in M variables, while the iterative solution method computes unique good solutions alone [24]. Other approaches offer the absolute hodograph winding number as the criterion for finding the unique solution [27,28].

Accurate estimation of the contour error is one of the crucial factors in the following contouring problems. In fact, several contour-error estimation algorithms that can be used in high speed contouring applications have been proposed [29–34]. These existing approaches can be used to estimate the contour error for linear, circular, and arbitrary tool-paths. In this paper, the contour error is computed using the method proposed by Erkorkmaz et al. [34]. This contour error estimation method is suitable for arbitrary tool paths and does not require analytical knowledge of the tool path. The contour error is specified at various regions on the actual tool path to calculate the shortest orthogonal distance between the reference tool path and the actual tool position.

The C^2 PH quintic spline curves and their interpolation are the focus of this paper. To construct the C^2 PH quintic spline curves, a uniform knot sequence is used. For solving the system of quadratic equations, the Newton–Raphson algorithm and the method of selecting the starting point proposed by Farouki et al. [24] are employed. In addition, the *S*-curve motion planning architecture with variable feedrate for a planar C^2 PH quintic spline curve is developed. To evaluate the effectiveness of the proposed interpolation algorithm, several closed C^2 PH quintic spline curve contouring tasks have been conducted.

The rest of the paper is organized as follows: In Section 2, the *B*-spline curves, along with the nodal points on the cubic *B*-spline curves, are presented. Section 3 summarizes the system of equations that define C^2 PH quintic interpolating splines including the choices of end conditions and the appropriate starting point in the Newton–Raphson method. In Section 4, real-time interpolations using the PH quintic curves are introduced, and the *S*-curve motion planning architecture with variable feedrate for a planar C^2 PH quintic spline curve is proposed. The performance evaluations of the C^2 PH quintic spline curves with variable feedrate are given in Section 5. Also, the experimental results are presented to demonstrate the feasibility of the proposed parametric interpolator. Finally, Section 6 concludes the paper.

2. Review on *B*-spline curves

The *B*-spline curve of degree p defined by given $n+1$ control points, $P_0, P_1, \ldots, P_n$, and the knot vector, $U = \{u_0, u_1, \ldots, u_m\}$, is:

$$c(u) = \sum_{k=0}^{n} N_{k,p}(u) P_k, \tag{1}$$

where $N_{k,p}(u)$'s are the *B*-spline basis functions of degree p described by:

$$N_{k,p}(u) = \frac{u - u_k}{u_{k+p} - u_k} N_{k,p-1}(u) + \frac{u_{k+p+1} - u}{u_{k+p+1} - u_{k+1}} N_{k+1,p-1}(u), \tag{2}$$

$$N_{j,0}(u) = \begin{cases} 1 & \text{if } u \in [u_j, u_{j+1}) \\ 0 & \text{otherwise.} \end{cases} \tag{3}$$

The De Cox–Boor's algorithm [35,36] can be used to determine the point on a *B*-spline curve corresponding to a specific parameter value, u. Hence, one can easily find the nodal points, which are the points on the *B*-spline curve corresponding to the specified knot points, $u_0, u_1, \ldots, u_m$, with $m = n + p + 1$. Jahanpour et al. [23] have presented the closed form formulation to evaluate the nodal points on the NURBS curves of degree 3. In their work, the following uniform knots have been adopted: $u_0 = u_1 = u_2 = u_3 = 0$, $u_k = k - 3$ for $k = 4, \ldots, n$, and $u_{m-3} = u_{m-2} = u_{m-1} = u_m = n - 2$.

Also, the nodal points have been described, as follows, by [23]:

$$\begin{aligned} q_0 &= c(u_3) = P_0, \\ q_1 &= c(u_4) = 1/A\,(3w_1P_1 + 7w_2P_2 + 2w_3P_3)\,, \\ q_{k-3} &= c(u_k) = 1/B\,(w_{k-3}P_{k-3} + 4w_{k-2}P_{k-2} + w_{k-1}P_{k-1})\,, \quad \text{for } k = 5, \ldots, n-1, \\ q_{n-3} &= c(u_n) \\ &= 1/C\,(2w_{n-3}P_{n-3} + 7w_{n-2}P_{n-2} + 3w_{n-1}P_{n-1})\,, \\ q_{n-2} &= c(u_{n+1}) = P_n, \end{aligned} \tag{4}$$

where $w_0, w_1, \ldots, w_n$ are the weights corresponding to the control points $P_0, P_1, \ldots, P_n$, respectively. Also, $A = 3w_1 + 7w_2 + 2w_3$, $B = w_{k-3} + 4w_{k-2} + w_{k-1}$, and $C = 3w_{n-1} + 7w_{n-2} + 2w_{n-3}$. Further details on computing the *B*-spline basis functions and the nodal points can be found in [23].

Regarding all weights to be equal to 1 in Eq. (4), the nodal points are computed by the following equation for the case of a cubic *B*-spline curve via Eq. (1).

$$
\begin{aligned}
&q_0 = c(u_3) = P_0,\\
&q_1 = c(u_4) = (3P_1 + 7P_2 + 2P_3)/12,\\
&q_{k-3} = c(u_k)\\
&\quad = (P_{k-3} + 4P_{k-2} + P_{k-1})/6, \quad \text{for } k = 5, \ldots, n-1,\\
&q_{n-3} = c(u_n) = (2P_{n-3} + 7P_{n-2} + 3P_{n-1})/12,\\
&q_{n-2} = c(u_{n+1}) = P_n.
\end{aligned} \tag{5}
$$

In this paper, to construct the closed cubic B-spline curves, cyclic interpretation of the control points is adopted. That is, the first p and last p control points are wrapped, i.e. $P_0 = P_{n-p+1}, P_1 = P_{n-p+2}, \ldots, P_{p-2} = P_{n-1}$ and $P_{p-1} = P_n$.

3. PH spline curves

The complex representation for a planar PH curve can be expressed as $r(\xi) = x(\xi) + iy(\xi)$, where $\xi \in [0, 1]$ is a real parameter [9]. $r(\xi)$ is a PH curve, if there exist polynomials, $u(\xi), v(\xi)$, such that its derivative, i.e. hodograph, $r'(\xi) = w^2(\xi)$, satisfies:

$$
\begin{aligned}
&x'(\xi) = u^2(\xi) - v^2(\xi),\\
&y'(\xi) = 2u(\xi)v(\xi),\\
&\sigma(\xi) = u^2(\xi) + v^2(\xi),
\end{aligned} \tag{6}
$$

where $\sigma(\xi) = \sqrt{x'^2(\xi) + y'^2(\xi)} = \left|\frac{d(r(\xi))}{d(\xi)}\right|$ is the rate of change of $r(\xi)$, with respect to the curve parameter, ξ.

3.1. C^2 PH quintic spline equations

We refer a C^2 PH spline to the connected PH curves that interpolate the nodal points of the corresponding cubic B-spline curve. In fact, the open/closed C^2 PH quintic spline associated with given control points, $P_0, P_1, \ldots, P_n$, and a knot vector, $U = \{u_0, u_1, \ldots, u_m\}$, is defined to be the good PH spline interpolant to the $n-1$ nodal points, $q_k = c(u_{3+k}),\ k = 0, \ldots, M = n-2$ of the cubic B-spline curve, specified by the given control polygon and knots [20,24].

The interpolation of the above $n-1$ nodal points begins by writing the hodograph of the PH quintic segment, $r_i(\xi), \xi \in [0, 1]$, of the spline curve, between points q_{i-1} and q_i. The polynomial, $w_i(\xi) = u_i(\xi) + iv_i(\xi)$, related to the $r_i(\xi)$ must be quadratic. Expressed in Bernstein form, the corresponding hodograph in complex form is:

$$
\begin{aligned}
r'_i(\xi) = \Bigg[&\frac{1}{2}(z_{i-1} + z_i)(1-\xi)^2\\
&+ z_i 2(1-\xi)\xi + \frac{1}{2}(z_i + z_{i+1})\xi^2\Bigg]^2.
\end{aligned} \tag{7}
$$

The continuity conditions for consecutive spans i and $i+1$ are: $r'_i(1) = r'_{i+1}(0)$, and $r''_i(1) = r''_{i+1}(0)$. Expanding Eq. (7) and substituting it into the interpolation condition integral, $\int_0^1 r'_i(\xi)d\xi = q_i - q_{i-1}$, by taking $r_i(0) = q_{i-1}$ as the integration constant, will yield the following equation:

$$
\begin{aligned}
f_i(z_{i-1}, z_i, z_{i+1}) = {}& 3z_{i-1}^2 + 27z_i^2 + 3z_{i+1}^2 + z_{i-1}z_{i+1}\\
&+ 13z_{i-1}z_i + 13z_i z_{i+1} - 60\Delta q_i = 0,
\end{aligned} \tag{8}
$$

where $\Delta q_i = q_i - q_{i-1}$ for $i = 1, \ldots, M$. However, the first and last equations, i.e. $f_1(z_1, \ldots, z_M) = 0$ and $f_M(z_1, \ldots, z_M) = 0$, must be modified or additional equations must be introduced through the end conditions discussed in the following subsection.

3.2. End conditions

If derivatives $d_i = r'_1(0)$ and $d_f = r'_M(1)$ at the end-nodal points, q_0 and q_M, are specified, the interpolation equations, i.e. Eq. (8), hold for all segments, $i = 1, \ldots, M$, and interpolation of the derivatives, d_i, d_f, yields two further equations:

$$
\begin{aligned}
&f_0(z_0, z_1) = (z_0 + z_1)^2 - 4d_i = 0,\\
&f_{M+1}(z_M, z_{M+1}) = (z_M + z_{M+1})^2 - 4d_f = 0.
\end{aligned} \tag{9}
$$

Using the above two equations and Eq. (8), total $M+2$ equations, i.e. $f_0 = 0, \ldots, f_{M+1} = 0$ (in $M+2$ complex variables, i.e. $z_0, \ldots, z_{M+1}$) are used to solve for the open C^2 PH quintic spline.

For the closed C^2 PH quintic spline, the end conditions $q_M = q_0$, $r'_M(1) = r'_1(0)$ and $r''_M(1) = r''_1(0)$ should be satisfied. To this end, Eq. (7) is replaced by the following relations [24]:

$$
\begin{aligned}
r'_1(\xi) = \Bigg[&\frac{1}{2}(\pm z_M + z_1)(1-\xi)^2 + z_1 2(1-\xi)\xi\\
&+ \frac{1}{2}(z_1 + z_2)\xi^2\Bigg]^2,\\
r'_M(\xi) = \Bigg[&\frac{1}{2}(z_{M-1} + z_M)(1-\xi)^2 + z_M 2(1-\xi)\xi\\
&+ \frac{1}{2}(z_M \pm z_1)\xi^2\Bigg]^2.
\end{aligned} \tag{10}
$$

Therefore, the first and last equations of the system described by Eq. (8) become:

$$
\begin{aligned}
f_1(z_1, \ldots, z_M) = {}& 3z_M^2 + 27z_1^2 + 3z_2^2 \pm z_M z_2 \pm 13z_M z_1\\
&+ 13z_1 z_2 - 60\Delta q_1 = 0,\\
f_M(z_1, \ldots, z_M) = {}& 3z_{M-1}^2 + 27z_M^2 + 3z_1^2 \pm z_{M-1}z_1\\
&+ 13z_{M-1}z_M \pm 13z_M z_1 - 60\Delta q_M = 0.
\end{aligned} \tag{11}
$$

Note that the same choice of sign must be used in f_1 and f_M in Eq. (11) and either choice can result in a "good" solution [24].

In order to solve the system equation described by Eq. (8) with above end conditions, numerical methods should be used. The Newton–Raphson iteration algorithm can be employed to compute the PH spline, from an appropriate starting approximation. In this paper, the starting approximation is calculated using the method developed in [24] in which the starting approximation to the solution is estimated by setting $z_{i-1} = z_i = z_{i+1}$ in Eq. (8):

$$
z_i^2 = \Delta q_i \quad \text{for } i = 1, \ldots, M. \tag{12}
$$

There are two choices for each z_i. Taking $\mathrm{Re}(z_1) > 0$, subsequent choices are made to minimize $|z_i - z_{i-1}|$. Further details on using the Newton–Raphson iteration method to solve Eq. (8) with appropriate end conditions can be found in [20,24]. Figure 1 shows a closed C^2 PH quintic spline curve computed by the Newton–Raphson iteration method. The "Butterfly" trajectory shown in Figure 1 is associated with a large control polygon of 50 discrete control points specified by small circles in Figure 1.

4. C^2 PH quintic spline curve interpolator

Real-time interpolation by PH quintic curves was developed by Farouki and Sagar [10] in 1996. They firstly presented formulations and analyzed where the feedrate on the PH curve is constant or specified as a linear/quadratic function of the

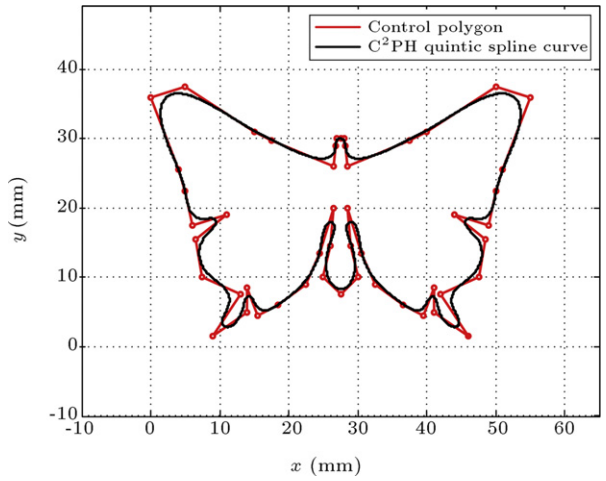

Figure 1: A "Butterfly" as a closed C^2 PH quintic spline curve (associated with 50 discrete control points) computed by the Newton–Raphson iteration method.

arc length. Later, Tsai et al. [14] introduced the PH curve interpolators with time-dependent feedrates in 2001. The real-time interpolation by PH quintic curves, with variable and constant federates, is first briefly reviewed in the following. Then, the *S*-curve motion planning architecture, with variable feedrate for a planar C^2 PH quintic spline curve, is proposed.

4.1. Time-dependent feedrate

Consider a time-dependent feedrate function, $V(t)$ for $t \in [0, T]$, imposed on the PH curve in which $V(t) = \dot{F}(t)$. Thus, the arc length is determined as $s(\xi) = F(t)$. Accordingly, for a sampling interval, Δt, the parameter values, $\xi_1, \xi_2, \ldots$, at times $\Delta t, 2\Delta t, \ldots$ are computed by the following equation:

$$s(\xi_k) = F(k\Delta t), \quad k = 0, 1, \ldots \tag{13}$$

Eq. (13) has a unique real root for each k. The value of ξ_k can be computed by the Newton–Raphson method in several iterations [14]:

$$\xi_k^{(r)} = \xi_k^{(r-1)} - \frac{s(\xi_k^{(r-1)}) - F(k\Delta t)}{\sigma(\xi_k^{(r-1)})}, \quad r = 1, 2, \ldots, \tag{14}$$

with starting approximation, $\xi_k^{(0)} = \xi_{k-1}$.

The case where V is a polynomial of t is a particularly simple form of variable feedrate, which is very useful in achieving smooth feed accelerations from rest (or feed decelerations to rest). Using the normalized time variable, $\tau = t/T$, and expressing $V(t)$ in the Bernstein basis form on the unit interval, $\tau \in [0, 1]$, we have:

$$V(\tau) = \sum_{k=0}^{n} v_k b_k^n(\tau) \tag{15}$$

where $b_k^n(\tau) = \binom{n}{k}(1-\tau)^{n-k}\tau^k$ and v_k are the Bernstein-basis functions and coefficients, respectively.

Given a polynomial, V, of odd degree, n, in Eq. (15), one can define a feedrate profile that matches $V = V_i$ for $t \leq 0$ and $V = V_f$ for $t > T$, with $C^{(n-1)/2}$ continuity. In order to obtain smooth motion transition between different phases along the path, and also ensure continuity of both the feed acceleration/deceleration and feed jerk, the *S*-curve C^1 cubic and C^2 quintic profiles are preferred, rather than the C^0 linear one [14]. One can easily find the appropriate Bernstein coefficients, v_k, for the C^1 cubic (or C^2 quintic) feed acceleration/deceleration. Figure 2 shows the C^1 cubic and C^2 quintic variable feedrate acceleration profiles defined by Eq. (15), when $V_i = 0$. Further details on selecting v_k for the acceleration and deceleration phases can be found in [14].

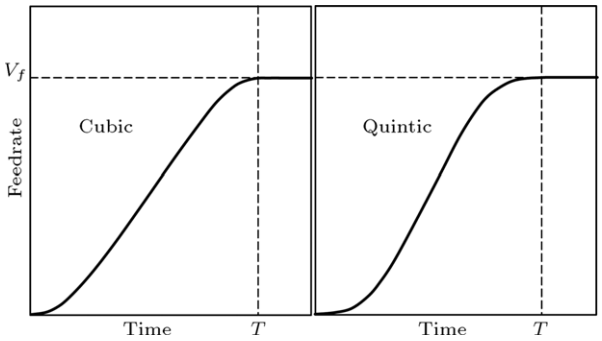

Figure 2: Feed accelerations from $V = 0$ for $t \leq 0$ to $V = V_f$ for $t \geq T$ using C^1 cubic, and C^2 quintic variable feedrates defined by Eq. (15) [14].

4.2. Constant feedrate

For the case of constant feedrate, the arc length is determined as $s(\xi_k) = k\Delta s_0$, where $\Delta s_0 = V_f \Delta t$ is the arc length in iteration k, and V_f is the constant feedrate. The desired sequence of parameter values, i.e. ξ_k, is computed by the Newton–Raphson method in several iterations:

$$\xi_k^{(r)} = \xi_k^{(r-1)} - \frac{s(\xi_k^{(r-1)}) - k\Delta s_0}{\sigma(\xi_k^{(r-1)})}, \quad r = 1, 2, \ldots. \tag{16}$$

The initial approximation for Eq. (16) is given by [10]:

$$\xi_k^{(0)} = \xi_{k-1} + \frac{\Delta s_0}{\sigma(\xi_{(k-1)})}. \tag{17}$$

4.3. The modified motion planning along the C^2 PH quintic spline curves

According to the aforementioned PH quintic curve interpolators, the modified motion planning, consisting of variable and constant feedrate profiles, for interpolating a C^2 PH quintic spline curve, is proposed and elaborated in the following:

1. Acceleration from full stop to the constant feedrate on the first PH quintic segment, $r_1(\xi)$, during the acceleration period $[0, T]$: In this phase of motion, the C^1 cubic feedrate acceleration along the PH quintic segment, $r_1(\xi)$, is imposed.
2. Constant velocity: This phase of motion starts from the end of the acceleration period along the PH quintic segment, $r_1(\xi)$, and ends at the beginning of the deceleration period along the PH quintic segment, $r_M(\xi)$. The C^2 PH quintic spline curve is interpolated by the constant feedrate of V_f in this phase.
3. Deceleration from the PH quintic segment, $r_M(\xi)$, with constant velocity to full stop: The C^1 cubic feedrate deceleration along the last PH quintic segment, $r_M(\xi)$, is imposed during this phase.

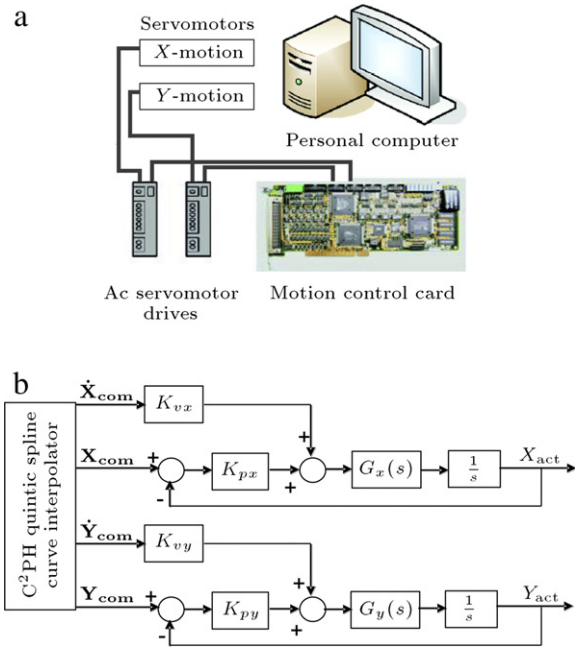

Figure 3: Experimental hardware and the block diagram of the servo controller used in the experiments. (a) Experimental hardware; and (b) block diagram of the servo controller.

5. Experiment setup and results

5.1. Experimental setup

In this paper, two AC servomotors are employed for the X- and Y-axes motions, where the servomotors are equipped with incremental encoders (2500×4 pulses/rev) for position feedback. Both servo drives are set to the velocity mode throughout the experiments. All the control algorithms are implemented using a PMC32-6000 motion control equipped with a high performance DSP-TI TMS320C32 floating point processor. For each axis, a simple position loop controller with a velocity command feed-forward is used to reduce the tracking error. The hardware and the control block diagram used in the experiments are shown in Figure 3. The input commands computed by the C^2 PH quintic spline interpolator, i.e. X_{com} (Y_{com}) and $\dot{X}_{\text{com}}$ ($\dot{Y}_{\text{com}}$), are the desired position and velocity commands for the $X(Y)$ axis, respectively. K_{px}, K_{py} are the position loop gains and K_{vx}, K_{vy} are the feed-forward gains. Also, X_{act} and Y_{act} in Figure 3(b), represent the actual positions for the X axis and Y axis, respectively.

The transfer function of the controlled plant from the velocity command input to the position output are obtained using the dynamic analyzer, HP3563A, for both motions of the X- and Y-axes respectively as follows [37]:

$$G_x = \frac{35.8958}{1 + 0.0033185s} \left(\frac{\text{rad/s}}{\text{V}}\right),$$

and:

$$G_y = \frac{39.2008}{1 + 0.0042222s} \left(\frac{\text{rad/s}}{\text{V}}\right).$$

Based on the measured transfer functions, G_x and G_y, one can determine the appropriate gain of the position loop controller, as shown in Figure 3(b), due to the specified bandwidth, which will be set to $K_{px} = 62\ \text{s}^{-1}$, $K_{py} = 47\ \text{s}^{-1}$, $K_{vx} = K_{vy} = 0.57$ for experimental study. The different settings for K_{px} and K_{py} are due to the fact that the loads for the X- and Y-axes are different. The above controller gains have been tuned, such that the best possible contour following performance is achieved in the experiments.

In the following, the proposed interpolation algorithm is implemented for two cases of the closed C^2 PH quintic spline curves and the performance of the proposed approach is also analyzed and discussed.

5.2. Case studies

In the following, two closed C^2 PH quintic spline curves are used for high speed contouring tasks in the experiments. One is the "Heart" curve and the other is the "Star" curve. The control points for constructing these two curves are selected as follows:

"*Heart*" *curve*:

$$P_0 = -20 - 50i, \quad P_1 = 0 + 5i, \quad P_2 = 0 - 5i,$$
$$P_3 = -20 + 50i, \quad P_4 = 40 + 50i, \quad P_5 = 75 - 5i,$$
$$P_6 = 75 + 5i, \quad P_7 = 40 - 50i, \quad P_8 = P_0,$$
$$P_9 = P_1, \quad P_{10} = P_2.$$

"*Star*" *curve*:

$$P_0 = 46.8 + 78i, \quad P_1 = 30 + 48i, \quad P_2 = 54i,$$
$$P_3 = 30 + 30i, \quad P_4 = 18, \quad P_5 = 48 + 30i,$$
$$P_6 = 78, \quad P_7 = 66 + 30i, \quad P_8 = 96 + 54i,$$
$$P_9 = 66 + 48i, \quad P_{10} = 49.2 + 78i,$$
$$P_{11} = P_0, \quad P_{12} = P_1, \quad P_{13} = P_2.$$

The above control points give the C^2 PH B-spline curves containing eight PH quintic segments for the "Heart" curve and eleven PH quintic segments for the "Star" curve. The total curve length computed for the "Heart" and the "Star" curves are $S_{\text{heart}} = 289.7626$ mm and $S_{\text{star}} = 239.6265$ mm, respectively. Additionally, the arc length of the first and the last PH quintic segments of the "Heart" curve are $S_{1\text{heart}} = 12.229$ mm and $S_{8\text{heart}} = 36.6574$ mm, respectively. While, those arc lengths for the "Star" curve are $S_{1\text{star}} = 19.4226$ mm and $S_{1\text{star}} = 25.6213$ mm.

Each contouring task is conducted under two different motion planning schemes proposed in Section 4, so as to evaluate the performance of the proposed approach. In particular, two different settings for variable feedrate profiles in Figure 2 are used: $V_f = 100$ mm/s, $T = 0.12$ s and $V_f = 120$ mm/s, $T = 0.12$ s. From Figure 2, the acceleration (deceleration) curve length traveled by C^1 cubic feedrate acceleration (deceleration) is given by $S_{\text{acc/dec}} = V_f \times T/2$. Thus, for the cases of $V_f = 100$ mm/s and $V_f = 120$ mm/s, only 6 mm and 7.2 mm of the first and the last PH quintic segments of the curve (with $S_{1\text{heart}}$, $S_{8\text{heart}}$, $S_{1\text{star}}$, and $S_{11\text{star}}$) are traveled, respectively. Note that in both interpolation algorithms and experiments, the sampling period, Δt, is set to 1 ms.

Using the above parameters for the proposed motion planning, the C^2 PH quintic B-spline curve interpolator computes the feedrate command required for each contouring task in the experiment. For example, the feedrate profile associated with $V_f = 100$ mm/s and $T = 0.12$ s for the "Heart" contouring task is shown in Figure 4. The X and Y feedrate components are also depicted as dashed curves in Figure 4. As can be seen in Figure 4, the feedrate command generated by the proposed interpolator is not only able to achieve the smooth motion transition between different phases along the path but also to avoid any fluctuations in the desired feedrate.

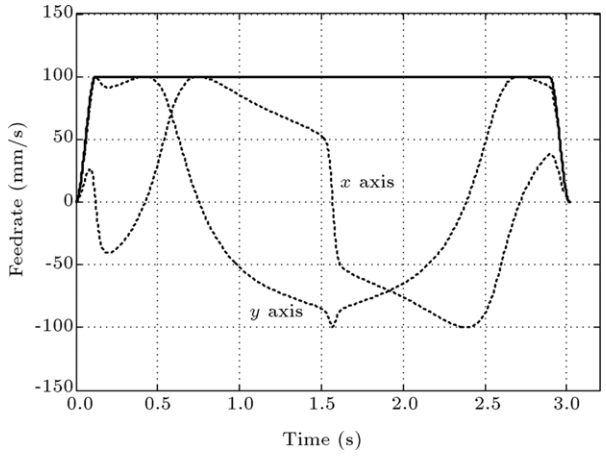

Figure 4: Feedrate command used in the experiments generated by the proposed interpolator for the "Heart" contouring task with $V_f = 100$ mm/s and $T = 0.12$ s.

5.3. Experimental results

"Heart" contouring

The experimental results for the "Heart" contouring task with $V_f = 100$ mm/s are given in Figure 5. The contouring motion started from the point $q_0 = -3.33 - 5.83i$ mm and traveled in a clockwise direction. The tracking performance is illustrated in Figure 5(a). It can be observed that the actual trajectory matches the desired one closely. The nonlinear phenomenon or physical constraints, such as friction and actuator saturation, causes the contour error. As can be seen in Figure 5(b), the maximum contour error is 0.168 mm, which occurred at the turning point shown in the inset of Figure 5(a). The curvature profile is shown in Figure 5(c), where the amount of the curvature at the turning point is 0.217 mm^{-1}, which differs by a small amount of 0.55%, with respect to the desired tool path. Figure 5(b) and (c) show that the contour error at the point with the largest curvature is larger than that for the other smoother portions of the curve. In fact, in the vicinity of the turning point with largest variations in the curvature, there are sudden changes of direction on axis movements, which result in the maximum contour error occurring at the turning point. Furthermore, the amount of this maximum error is also affected by the friction and actuator saturation from the biaxial reverse motion at the turning point with the largest curvature. Although there is no systematic way for minimizing the error between the desired and the experimental tool path, use of the variety of alternative control schemes may decrease the contour error [38].

To compare the actual feedrate with the desired feedrate command along the curve, the actual feedrate profile and the desired feedrate profile for this case are given in Figure 6. Although the desired feedrate profile does not have any fluctuations, the sudden change of motion in the X direction results in a small variation in the actual feedrate profile. The maximum variation in the actual feedrate profile is about 2.5%, as shown in the inset of Figure 6, which is related to the mentioned turning region with the largest curvature on the "Heart" curve.

The experimental results for the "Heart" contouring task with $V_f = 120$ mm/s are given in Figure 7. It can be observed that the actual trajectory also matches the desired one closely, as shown in Figure 7(a), where the maximum contour error is 0.218 mm as indicated by Figure 7(b). For this case, the

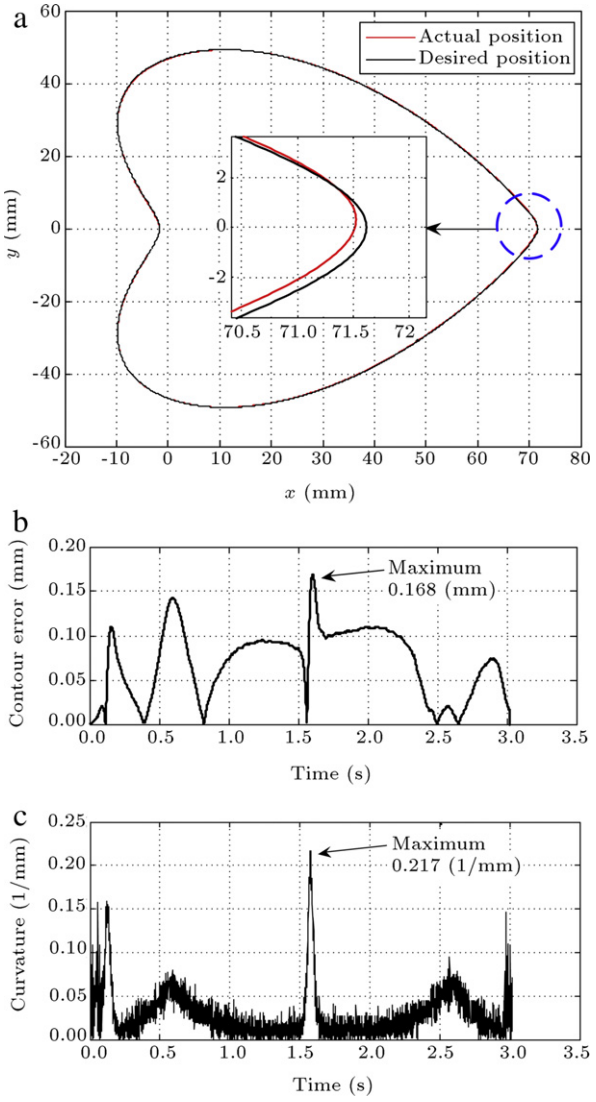

Figure 5: Experimental results for the "Heart" contour-following task with $V_f = 100$ mm/s. (a) Position along the "Heart" curve using the proposed interpolator; (b) contour error for "Heart" tracking; and (c) curvature profile.

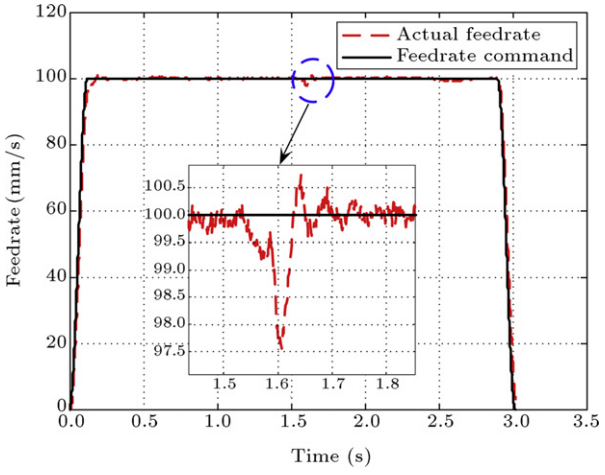

Figure 6: Feedrate profile along the "Heart" curve with $V_f = 100$ mm/s using C^2 PH spline curve interpolator.

Table 1: Experimental results for the "Heart" contouring task.

Motion planning parameters	Total machining time (s)	Maximum actual feedrate fluctuation (%)	Maximum actual curvature (1/mm)	Maximum contour error (mm)
$V_f = 100$ mm/s, $T = 0.12$ s	3.019	2.5	0.217	0.168
$V_f = 120$ mm/s, $T = 0.12$ s	2.536	3.49	0.218	0.218

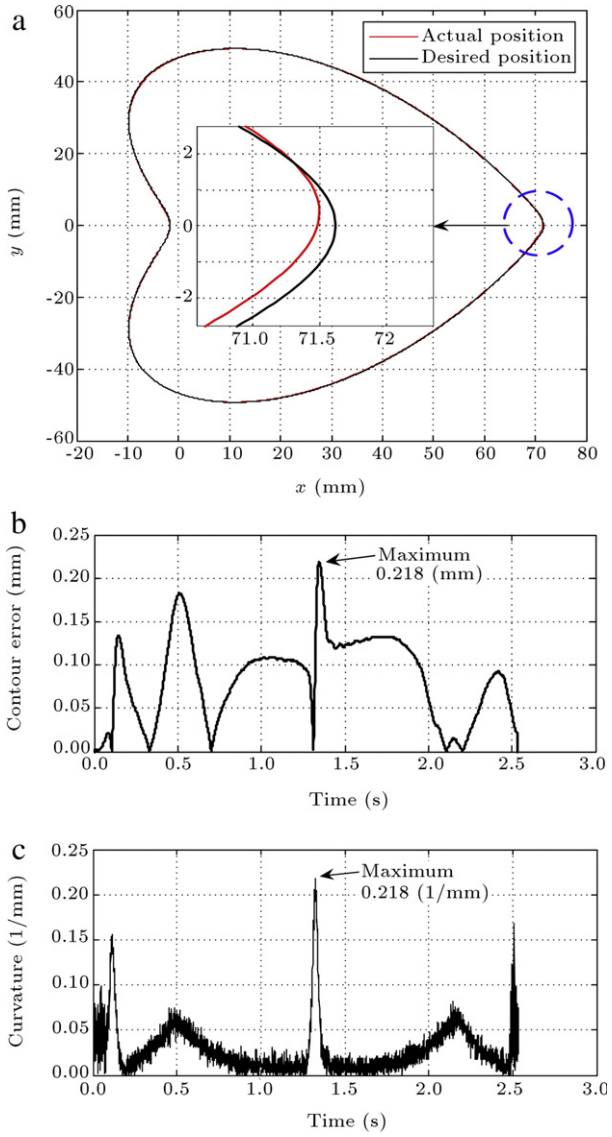

Figure 7: Experimental results for the "Heart" contouring task with $V_f = 120$ mm/s. (a) Position along the "Heart" curve using the proposed interpolator; (b) contour error for "Heart" tracking; and (c) curvature profile.

maximum variation in the actual feedrate profile that occurred at the turning region with a curvature of 0.218 mm^{-1} is 3.49% as shown in Figure 7(c). Table 1 summarizes the experimental results of the "Heart" contouring task with two different cases for the velocity planning.

"Star" contouring

The experimental results for the "Star" contouring task with $V_f = 100$ mm/s and $V_f = 120$ mm/s are given in Figures 8 and 9, respectively. In particular, the "Star" contouring motion started from the point $q_0 = 27.8 + 54i$ mm and traveled in a counter-clockwise direction. The tracking performance is illustrated in Figures 8(a) and 9(a), while, the contour error is shown in Figures 8(b) and 9(b). As can be seen in Figures 8(b) and 9(b), the maximum contour error for the case of $V_f = 100$ mm/s is 0.202 mm, and the maximum contour error for the case of $V_f = 120$ mm/s is 0.258 mm. The region that has the maximum corner error is enlarged in "Detail 1" in Figures 8(a) and 9(a). The curvature profiles obtained from the experimental data are shown in Figures 8(c) and 9(c), where the higher peaks of the contour error occurred at the blade regions of the "Star", which have higher curvature than the other portion of the "Star". Also, the lower peaks occurred at the concave region of the curve. The maximum curvature of the desired tool path is computed as 0.418 mm^{-1} for the last blade of the "Star" enlarged in Figures 8(a) and 9(a), as "Detail 2", and also the experimental results show that the curvature of the last blade is larger than the other blades of the "Star". In addition, the difference between

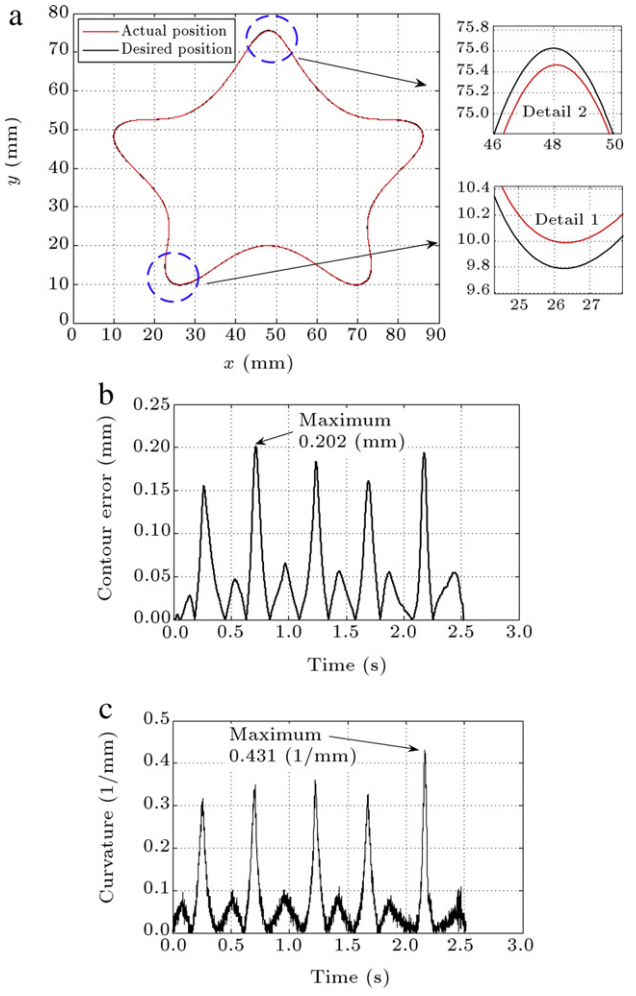

Figure 8: Experimental results for the "Star" contour-following task with $V_f = 100$ mm/s. (a) Position along the "Star" curve using the proposed interpolator; (b) contour error for "Star" tracking; and (c) curvature profile.

Table 2: Experimental results for the "Star" contouring task.

Motion planning parameters	Total machining time (s)	Maximum actual feedrate fluctuation (%)	Maximum actual curvature (1/mm)	Maximum contour error (mm)
$V_f = 100$ mm/s, $T = 0.12$ s	2.518	6.1	0.431	0.202
$V_f = 120$ mm/s, $T = 0.12$ s	2.119	6.32	0.444	0.258

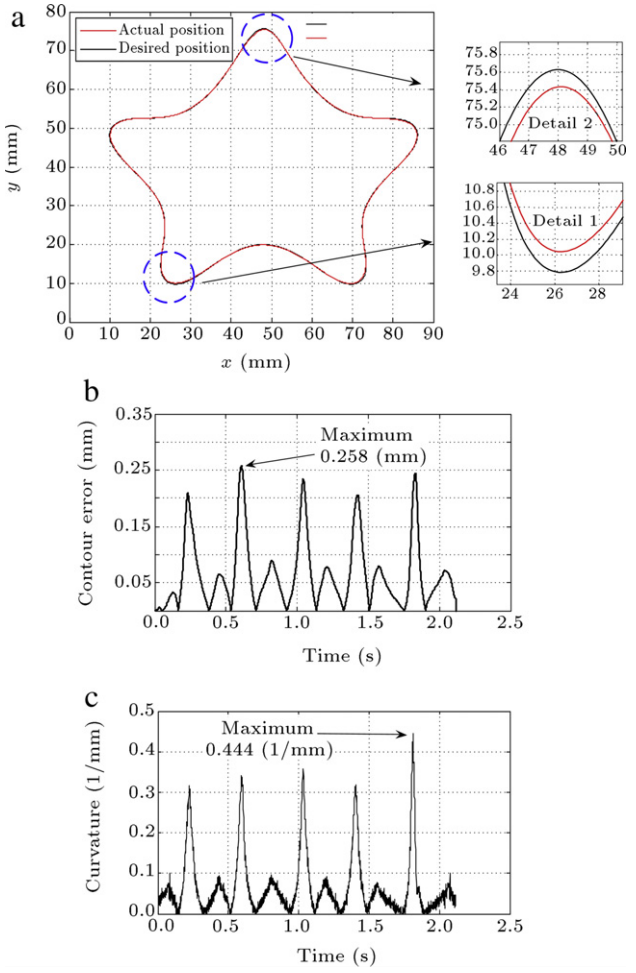

Figure 9: Experimental results for the "Star" contouring task with $V_f = 120$ mm/s. (a) Position along the "Star" curve using the proposed interpolator; (b) contour error for "Star" tracking; and (c) curvature profile.

the contour error around this blade and the maximum contour error is small. Table 2 summarizes the experimental results of the "Star" contouring task with two different cases of motion planning.

The experimental results listed in Tables 1 and 2 indicate that the proposed C^2 PH quintic *B*-spline curve interpolator is able to achieve a satisfactory tracking performance for variable feedrate control, even using a simple position loop controller.

6. Conclusions

This paper has proposed a C^2 PH quintic spline curve interpolator for a high speed contouring application. The PH spline curve inherits all the advantages of the PH curves and significant properties of the *B*-spline curves, so that it can be used to represent the complicated open and closed shapes used in the CAD/CAM systems. Using a combination of time-dependent and constant feedrates, the *S*-curve motion planning architecture, with variable federate, for a planar C^2 PH quintic spline curve, has also been developed. Accordingly, the developed toolpath interpolation yields an arc-length parameterized curve, which results in a feedrate command without any fluctuation. The proposed interpolation algorithm has been implemented for the "Heart" and the "Star" contouring tasks. Experimental results demonstrated that the proposed CNC interpolator is feasible for machining the parametric curves represented in the C^2 PH quintic spline form. Moreover, it is able to achieve a satisfactory contouring performance for variable feedrate control.

References

[1] Erkorkmaz, K. and Altintas, Y. "Quintic spline interpolation with minimal feed fluctuation", *Trans. ASME, J. Manuf. Sci. Eng*, 127(2), pp. 339–349 (2005).
[2] Wang, F.C. and Wright, P.K. "Open architecture controllers for machine tools, part 2: a real time quintic spline interpolator", *Trans. ASME, J. Manuf. Sci. Eng*, 120(2), pp. 425–432 (1998).
[3] Cheng, C.-W. and Tsai, M.-C. "Real-time variable feedrate NURBS curve interpolator for CNC machining", *Int. J. Adv. Manuf. Technol.*, 23(11–12), pp. 865–873 (2004).
[4] Sekar, M., Narayanan, V.N. and Yang, S.H. "Design of jerk boundedfeedrate with ripple effect for adaptive nurbs interpolator", *Int. J. Adv. Manuf. Technol.*, 37(5–6), pp. 545–552 (2008).
[5] Park, J., Nam, S. and Yang, M. "Development of a real-time trajectory generator for NURBS interpolation based on the two-stage interpolation method", *Int. J. Adv. Manuf. Technol.*, 26(4), pp. 359–365 (2005).
[6] Farouki, R.T. and Tsai, Y.F. "Exact Taylor series coefficients for variable-feedrate CNC curve interpolators", *Comput. Aided Geom. Des.*, 33(2), pp. 155–165 (2001).
[7] Tsai, M.-C. and Cheng, C.W. "A real-time predictor–corrector interpolator for CNC machining", *Trans. ASME, J. Manuf. Sci. Eng.*, 125(3), pp. 449–460 (2003).
[8] Farouki, R.T. and Sakkalis, T. "Pythagorean hodographs", *IBM J. Res. Dev.*, 34(5), pp. 736–752 (1990).
[9] Moon, H.P., Farouki, R.T. and Choi, H.I. "Construction and shape analysis of PH quintic Hermite interpolants", *Comput. Aided Geom. Des.*, 18(2), pp. 93–115 (2001).
[10] Farouki, R.T. and Sagar, S. "Real-time CNC interpolators for Pythagorean-hodograph curves", *Comput. Aided Geom. Des.*, 13(7), pp. 583–600 (1996).
[11] Farouki, R.T., Tsai, Y.F. and G F, Yuan "Contour machining of free-form surfaces with real-time PH curve CNC interpolators", *Comput. Aided Geom. Des.*, 16(1), pp. 61–76 (1999).
[12] Jahanpour, J. and Imani, B.-M. "Real-time P-H curve CNC interpolators for high speed cornering", *Int. J. Adv. Manuf. Technol.*, 39(3–4), pp. 302–316 (2008).
[13] Farouki, R.T., Manjunathaiah, J. and Yuan, G.F. "G codes for the specification of Pythagorean-hodograph tool paths and associated feedrate functions on open-architecture CNC machines", *Int. J. Mach. Tools Manuf.*, 39(1), pp. 123–142 (1997).
[14] Tsai, Y.F., Farouki, R.T. and Feldman, B. "Performance analysis of CNC interpolators for time-dependent feed rates along PH curves", *Comput. Aided Geom. Des.*, 18(3), pp. 245–265 (2001).
[15] Komanduri, R., Subramanian, K. and Turkovich, B.F. "High Speed Machining", *PED-12*, pp. 15–34, ASME, New York (1984).
[16] Smith, S. and Tlusty, J. "Current trends in high-speed machining", *Trans. ASME, J. Manuf. Sci. Eng.*, 119, pp. 664–666 (1997).
[17] Tlusty, J. "High-speed machining", *CIRP Ann.*, 42(2), pp. 733–738 (1993).
[18] Aigner, M., Sir, Z. and Juttler, B. "Evolution-based least-squares fitting using Pythagorean hodograph spline curves", *Comput. Aided Geom. Des.*, 24(6), pp. 310–322 (2007).

[19] Sir, Z. and Juttler, B. "Constructing acceleration continuous tool paths using Pythagorean hodograph curves", *Mech. Mach. Theory*, 40, pp. 1258–1272 (2005).
[20] Pelosi, F., Sampoli, M.L., Farouki, R.T. and Manni, C. "A control polygon scheme for design of planar C2 PH quintic spline curves", *Comput. Aided Geom. Des.*, 24(1), pp. 28–52 (2007).
[21] Albrecht, G. and Farouki, R.T. "Construction of C2 Pythagorean hodograph interpolating splines by the homotopy method", *Adv. Comput. Math.*, 5(4), pp. 417–442 (1996).
[22] Farouki, R.T., Manjunathaiah, J. and Jee, S. "Design of rational cam profiles with Pythagorean-hodograph curves", *Mech. Mach. Theory*, 33, pp. 669–682 (1998).
[23] Jahanpour, J., Tsai, M.-C. and Cheng, M.-Y. "High speed contouring control with NURBS-based C2 PH spline curves", *Int. J. Adv. Manuf. Technol.*, 49(5–8), pp. 663–674 (2010).
[24] Farouki, R.T., Kuspa, B.K., Manni, C. and Sestini, A. "Efficient solution of the complex quadratic tridiagonal system for C^2 PH quintic splines", *Numer. Algorithms*, 27(1), pp. 35–60 (2001).
[25] Mohyud-Din, S.T., Noor, M.A. and Noor, K.I. "Some relatively new techniques for nonlinear problems", *Math. Probl. Eng.*, 2009, p. 25 Article ID 234849 (2009), http://dx.doi.org/10.1155/2009/234849.
[26] Mohyud-Din, S.T. and Noor, M.A. "Homotopy perturbation method for solving partial differential equations", *J. Phys. Sci.*, 64a, pp. 157–170 (2009).
[27] Choi, H.I. and Kwon, S.H. "Absolute hodograph winding number and planar PH quintic splines", *Comput. Aided Geom. Des.*, 25(4–5), pp. 230–246 (2008).
[28] Choi, H.I., Farouki, R.T., Kwon, S.H. and Moon, H.P. "Topological criterion for selection of quintic Pythagorean-hodograph Hermite interpolants", *Comput. Aided Geom. Des.*, 25, pp. 411–433 (2008).
[29] Koren, Y. "Cross-coupled biaxial computer control for manufacturing systems", *J. Dyn. Syst. Meas. Control*, 102(4), pp. 265–272 (1980).
[30] Dong, J. and Stori, J.A. "Optimal feed-rate scheduling for high-speed contouring", *Proceedings of ASME-IMECE'03*, MED-42357 (2003).
[31] Cheng, M.-Y. and Lee, C.C. "Motion controller design for contour following tasks based on real-time contour error estimation", *IEEE Trans. Ind. Electron.*, 54(3), pp. 1686–1695 (2007).
[32] Koren, Y. and Lo, C.C. "Variable-gain cross-coupling controller for contouring", *Ann. CIRP*, 40(1), pp. 371–374 (1991).
[33] Erkorkmaz, K. and Altintas, Y. "High speed contouring control algorithm for CNC machine tools", *Proceedings of ASME Dynamic Sys Control Division, IMECE'98, DSC-64*, pp. 463–469 (1998).
[34] Erkorkmaz, K., Yeung, C.H. and Altintas, Y. "Virtual CNC system. Part II. High speed contouring application", *Int. J. Mach. Tools Manuf.*, 46(10), pp. 1124–1138 (2006).
[35] Cox, M.G. "The numerical evaluation of B-splines", *J. Inst. Math. Appl.*, 10, pp. 134–149 (1972).
[36] De Boor, C. "On calculating with B-splines", *J. Approx. Theory*, 6, pp. 50–62 (1972).
[37] Jahanpour, J., Tsai, M.-C., Cheng, M.-Y. and Liu, I.H. "Contour following using C^2 PH quintic spline curve interpolators", *Proceedings of the 18th IFAC World Congress*, 18 (1), pp. 9361–9366 (2011).
[38] Su, K. and Cheng, M.-Y. "Contouring accuracy improvement using cross-coupled control and position error compensator", *Int. J. Mach. Tools Manuf.*, 48, pp. 1444–1453 (2008).

Javad Jahanpour received a B.S. degree in Mechanical Engineering from Ferdowsi University of Mashhad (FUM), Iran, an M.S. degree in Applied Mechanical Engineering from Isfahan University of Technology (IUT), Iran, and a Ph.D. degree with first class Honours in Mechanical Engineering in 2008 from Ferdowsi University of Mashhad (FUM), Iran. From 2008 to 2009, he was Post-Doctoral researcher at National Cheng Kung University (NCKU), Taiwan. He is currently Assistant Professor in the Mechanical Engineering Department at the Islamic Azad University of Mashhad (IAUM). His research interests include trajectory generation and control motion problem with applications in robotics, vibration and CAD/CAM systems.